Cement & Concrete Composites 36 (2013) 56–64

Contents lists available at SciVerse ScienceDirect

Cement & Concrete Composites

journal homepage: www.elsevier.com/locate/cemconcomp

Nanostructural characterization of geopolymers by advanced beamline techniques

John L. Provis [a,*], Ailar Hajimohammadi [a], Claire E. White [a,b,c], Susan A. Bernal [a], Rupert J. Myers [a], Robert P. Winarski [d], Volker Rose [d,e], Thomas E. Proffen [b,f], Anna Llobet [b], Jannie S.J. van Deventer [a,g]

[a] Department of Chemical & Biomolecular Engineering, University of Melbourne, Victoria 3010, Australia
[b] Lujan Neutron Scattering Center, Los Alamos National Laboratory, Los Alamos, NM, USA
[c] Physics and Chemistry of Materials and Center for Nonlinear Studies, Los Alamos National Laboratory, Los Alamos, NM, USA
[d] Center for Nanoscale Materials, Argonne National Laboratory, Argonne, IL, USA
[e] Advanced Photon Source, Argonne National Laboratory, Argonne, IL, USA
[f] Powder Diffraction Group, Oak Ridge National Laboratory, Oak Ridge, TN, USA
[g] Zeobond Pty Ltd., P.O. Box 210, Somerton, Victoria 3062, Australia

ARTICLE INFO

Article history:
Received 31 January 2012
Received in revised form 6 July 2012
Accepted 17 July 2012
Available online 27 July 2012

Keywords:
Geopolymer
Alkali-activated binder
Synchrotron radiation
Neutron scattering
Nanostructure
Microstructure

ABSTRACT

This paper presents the outcomes of a series of beamline-based studies, the results of which are combined to provide a more detailed multiscale understanding of the structure and chemistry of geopolymer binders.

The range of beamline-based characterization techniques which have been applied to the study of geopolymer binders is increasing rapidly; although no single technique can provide a holistic view of binder structure across all the length scales which are of importance in determining strength development and durability, the synergy achievable through the combination of multiple beamline techniques is leading to rapid advances in knowledge in this area. Studies based around beamline infrared and X-ray fluorescence microscopy, *in situ* and *ex situ* neutron pair distribution function analysis, and nano- and micro-tomography, are combined to provide an understanding of geopolymer gel chemistry, nano- and microstructure in two and three dimensions, and the influences of seeded nucleation and precursor chemistry in these key areas.

The application of advanced characterization methods in recent years has brought the understanding of geopolymer chemistry from a point, not more than a decade ago, when the analysis of the detailed chemistry of the aluminosilicate binder gel was considered intractable due to its disordered ("X-ray amorphous") nature, to the present day where the influence of key compositional parameters on nanostructure is well understood, and both gel structure and reaction kinetics can be manipulated through methods including seeding, temperature variation, and careful mix design.

This paper therefore provides a review outlining the value of nanotechnology – and particularly nanostructural characterization – in the development and optimization of a new class of environmentally beneficial cements and concretes. Key engineering parameters, in particularly strength development and permeability, are determined at a nanostructural level, and so it is essential that gel structures can be analyzed and manipulated at this level; beamline-based characterization techniques are critical in providing the ability to achieve this goal.

1. Introduction

The detailed characterization of all cements (traditional and non-traditional) requires the application of advanced experimental techniques, due to the complex and locally disordered nature of most of the key chemical phases responsible for strength development and retention [1]. This is particularly the case for alkali-activated binders, where the binder is almost entirely lacking in coherent long-range ordering, and thus is intractable to analysis by classical diffractometry [2]. These binders are obtained by the reaction between an alkali source and a solid aluminosilicate powder, often metakaolin, fly ash and/or blast furnace slag, and are increasingly being utilized as a lower-CO_2 alternative to Portland cement in concrete production [3–5]. The increasing availability and capabilities of beamline-based instrumentation for the analysis of complex materials, at both synchrotron and neutron sources, is leading to major developments in this area at present. It is essential, in introducing a new class of construction materials, to be able to provide a detailed molecular-scale understanding of the reaction

* Corresponding author. Present address: Department of Materials Science and Engineering, University of Sheffield, Sheffield S1 3JD, United Kingdom. Tel.: +44 114 222 5490.
E-mail address: j.provis@sheffield.ac.uk (J.L. Provis).

0958-9465/$ - see front matter © 2012 Elsevier Ltd. All rights reserved.
http://dx.doi.org/10.1016/j.cemconcomp.2012.07.003

processes and chemical bonding environments which control its strength development (in terms of both rate and final strength) and durability, as a way to underpin the analysis of data obtained through (more widely available) bulk-scale standardized testing procedures. As the application of common laboratory-based analytical techniques to alkali-activated binders does not always provide a full understanding of detailed chemical structures and mechanisms due to the complexity and disordered nature of the key binder gel phases, it is important to generate a deeper level of understanding through the application of more advanced techniques, including beamline-based techniques as discussed in this brief review.

This paper will briefly summarize some advances which have been made recently in the understanding of alkali-activated binders based on the application of beamline-based characterization techniques. This is presented in the format of a review of some of the novel information which can be obtained by the different experimental techniques described, with the aim of stimulating further discussions and developments in related areas.

2. Results and discussion

2.1. Synchrotron infrared microscopy

Infrared microscopy beamlines, which are located at various synchrotron sources worldwide including the Australian Synchrotron [6], provide the opportunity to collect spatially-resolved infrared data for polished samples at a spatial resolution of approximately 10 μm. Infrared spectroscopy has been shown to be a particularly sensitive probe of the extent of formation and cross-linking of the binder gel in low-calcium alkali-activated materials [7–9], and these gels have been believed to form with a chemically heterogeneous structure depending on the relative rates and sites at which gel nucleation and growth processes can take place [10,11]. It therefore appears logical that analysis of gel structures by spatially-resolved infrared microscopy should prove instructive in understanding the influence of different synthesis parameters on the extent of gel heterogeneity. This has been proven to be the case in developing an understanding of the effect of differences in the availability of the binder-forming species silica [12] and alumina [13], where the combination of time-resolved (*in situ* attenuated total reflectance) and spatially resolved (synchrotron) infrared spectroscopy has provided powerful new insight. Fig. 1 shows an example of the results obtained by application of synchrotron infrared microscopy to a geopolymer derived by the reaction of geothermal silica and sodium aluminate, after 28 days of curing, with and without 0.5 wt.% of Al_2O_3 nanoparticles (565 m^2/g surface area) [14]. The data presented in Fig. 1 are the results of hierarchical clustering analysis of the infrared microscopy data; Fig. 1a and b show the clustered spectra representing each of the points on the sample, for the unseeded (a) and seeded (b) cases, and (c) and (d) show the distribution of the regions with each type of gel structure within a 100 μm × 125 μm region.

Fig. 1 demonstrates that synchrotron radiation-based infrared microscopy can aid in elucidating the effects of nucleation on the heterogeneous structure of geopolymer gels. While spatially averaged (i.e. laboratory-based) infrared results show similar spectra for seeded and unseeded samples which have been cured for more than three weeks [14], infrared microscopy shows marked differences in gel structure as a result of seeding.

In the dominant spectra ([1]yellow and orange) in the unseeded sample (Fig. 1a), there is a shoulder at about 1090 cm^{-1} which is assigned to unreacted geothermal silica [14], and which is much less prominent in the seeded sample. The maximum of the Si–O–T asymmetric stretch 'geopolymer' peak [8] also appears in two very distinct positions in the unseeded sample, either 945 cm^{-1} (in the black and brown spectra) or 975 cm^{-1} (yellow and orange spectra) – this separation is not visible in laboratory infrared analysis [7,14], which provides a spatially averaged view of the sample (either averaged throughout the bulk, when using the KBr pellet technique, or averaged over the surface layer when using attenuated total reflectance geometry), thus providing spectra which are a weighted average of the components visible in synchrotron infrared microscopy. In the seeded sample, this band is always observed at about 960 cm^{-1} in all spectra, showing a greater degree of homogeneity in the geopolymer gel in the seeded sample. This is an important result with consequences in geopolymer mix design for optimal gel structure and stability, and was not evident from the analysis of laboratory infrared spectroscopy data [14], highlighting the unique capabilities of the beamline-based technique in this instance.

2.2. In situ neutron pair distribution function analysis of geopolymer formation

Pair distribution function (PDF) analysis, which involves the generation of real-space structural information by the calculation of the Fourier transform of high-momentum transfer neutron or X-ray scattering data [15,16], is a powerful technique for the analysis of disordered materials. The disordered nature of the geopolymer binder phase is highly amenable to analysis by this technique, as has been discussed in recent reviews [1,17], and significant advances in the understanding of geopolymer nanostructure have been obtained by both X-ray [18,19] and neutron [20,21] pair distribution function analysis. *In situ* analysis of geopolymer formation has previously been undertaken by a variety of laboratory and beamline techniques, including in particular the use of *in situ* energy-dispersive X-ray diffractometry to provide direct kinetic information regarding gel structure formation using high-energy synchrotron radiation [22,23]. However, it is only recently that developments in instrumentation and data processing capabilities have enabled this process to be studied *in situ* while generating data sets of sufficient range and resolution to be amenable to PDF analysis. Both X-rays and neutrons have been used to study the formation of alkali-activated binder during *in situ* experiments; the X-ray results are reported elsewhere [24], while the neutron data were described in [21] and are summarized briefly here. Fig. 2 shows the evolution of geopolymer nanostructure as a function of reaction time (times as marked in Fig. 2a), where time zero was the time of mixing of a 'pure' metakaolin source (obtained by calcination of the reference kaolin clay KGa-1b) with a sodium silicate solution with molar ratio $SiO_2/Na_2O = 2.0$.

Fig. 2a shows that the geopolymer gel structure is highly disordered; atomic correlations beyond 3 Å are weak in the sample analyzed here. The most critical information obtained from Fig. 2 relates to the development of the gel structure, as seen in the (Si,Al)–O peak in Fig. 2b. The (Si,Al)–O bond length is seen to be shorter in the early-age geopolymer PDFs than in the precursor metakaolin, or in the 'final' (90-day) geopolymer gel. Residual metakaolin accounts for the shoulder at ~1.9 Å in the first 14 h [25,26]; the aluminum environment in this time period remains mostly in a metakaolin-like configuration, indicating that the bulk of the solid precursor is yet to dissolve. However, after 90 days this sample no longer contains a significant amount of undissolved metakaolin, which is visible in Fig. 2b as most of the aluminum has become IV-coordinated with Al–O correlations between ~1.75 and 1.8 Å.

[1] For interpretation of color in Figs. 1–4, the reader is referred to the web version of this article.

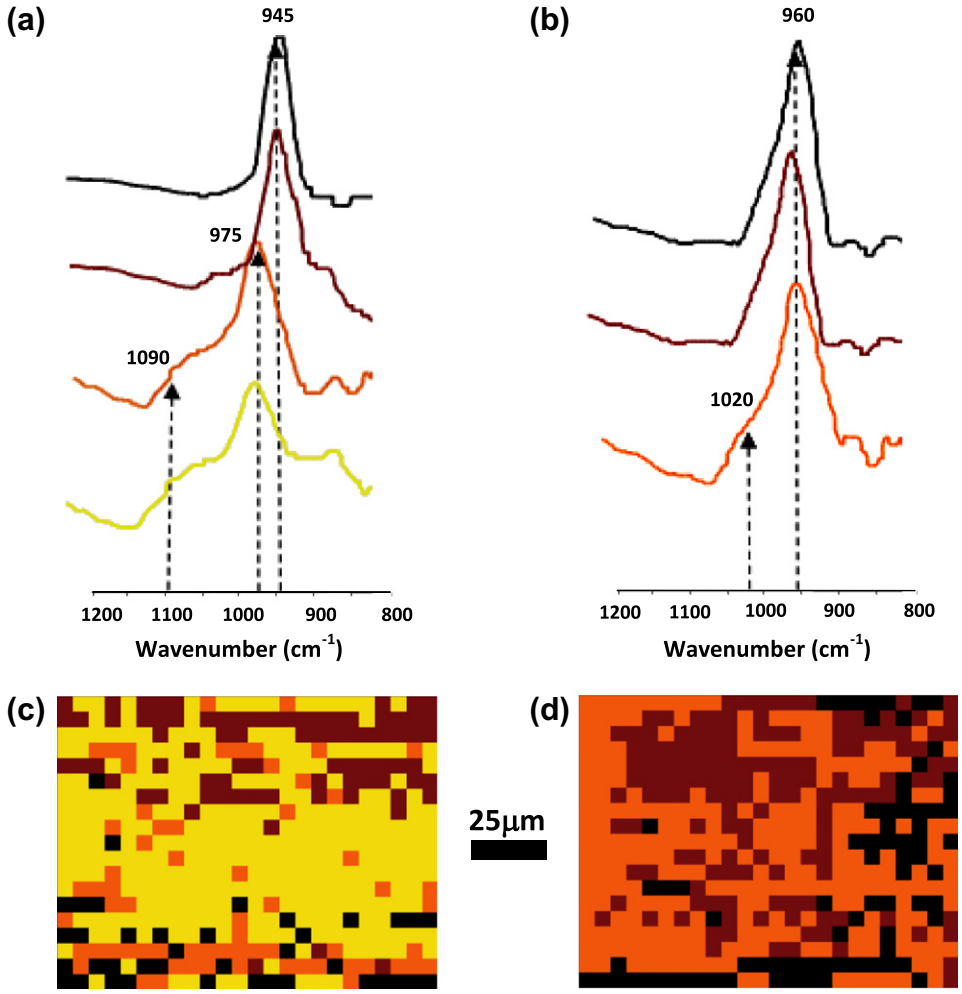

Fig. 1. Synchrotron infrared microscopy data for geothermal silica–sodium aluminate geopolymer binders, without (a and c) and with (b and d) 0.5 wt.% nano-Al_2O_3 seeding. Hierarchical clustering of the spectra obtained at each point results in the cluster spectra shown in (a) and (b), and the distributions of the spectra on the samples are shown in (c) and (d). Data from [14], collected using the Infrared beamline of the Australian Synchrotron, Clayton, Victoria, Australia, in attenuated total reflectance geometry using a diamond crystal probe.

Although the distinct Al–O shoulder in Fig. 2b changes minimally during the first 14 h, there is a variation in the distance at which the (Si,Al)–O correlation is a maximum. This is attributed to some of the aluminum being released from the metakaolin, then taking on IV-co-ordination in solution and in the newly-formed geopolymer. Between 14 h and 90 days there is a very notable change in the Al–O correlation, and the changes in the (Si,Al)–O correlation during this time are attributed to changes in both silicon and aluminum local environments during metakaolin dissolution and geopolymer gelation. By 90 days the sample has evolved to form a hardened binder material due to polymerization of the silicate and aluminate monomeric species from the solution, and the majority of the aluminum is bound in the geopolymer matrix and in IV-fold coordination [27,28].

Fig. 2c shows the O–D peak, which is considered equivalent to the O–H peak in non-deuterated samples, although possibly showing some subtle differences due to kinetic isotope effects and the additional mass of the D atom compared to H. The datasets up to 14 h are very similar, with a maximum at 0.955 Å, showing that the local structure of water in the geopolymer in the first 14 h of reaction is relatively unchanged, with a very small shift and slight sharpening observed at 90 days. This geopolymer has been seen to contain mobile water loosely held in large pores, with only <5% either physically bound in small pores or chemically bound as hydroxyl groups attached to the Si–Al framework structure [20]. This appears to be the case throughout the reaction process, with the slight changes observed between 14 h and 90 days attributed to the release of some of the initially bound hydroxyl (or in this case deuteroxyl) groups as additional molecular water during condensation reactions in the gel binder.

This information related to both framework and extra-framework species is difficult to directly access by standard laboratory experimental techniques, particularly related to disordered or 'X-ray amorphous' phases. The ability to collect such data *in situ* during reaction, or *ex situ* for sets of samples treated under different processing conditions, is particularly appealing in characterizing geopolymer binders, and is made available only through the development of highly specialized beamline facilities at advanced X-ray and neutron sources.

2.3. X-ray fluorescence microscopy

X-ray spectroscopy is often used in conjunction with electron microscopy to provide localized compositional information for heterogeneous samples such as alkali-activated binder materials [11,29–31], but the spatial resolution of this technique in application to geopolymers is limited to some extent by the relatively large interaction volumes observed when high-energy electron

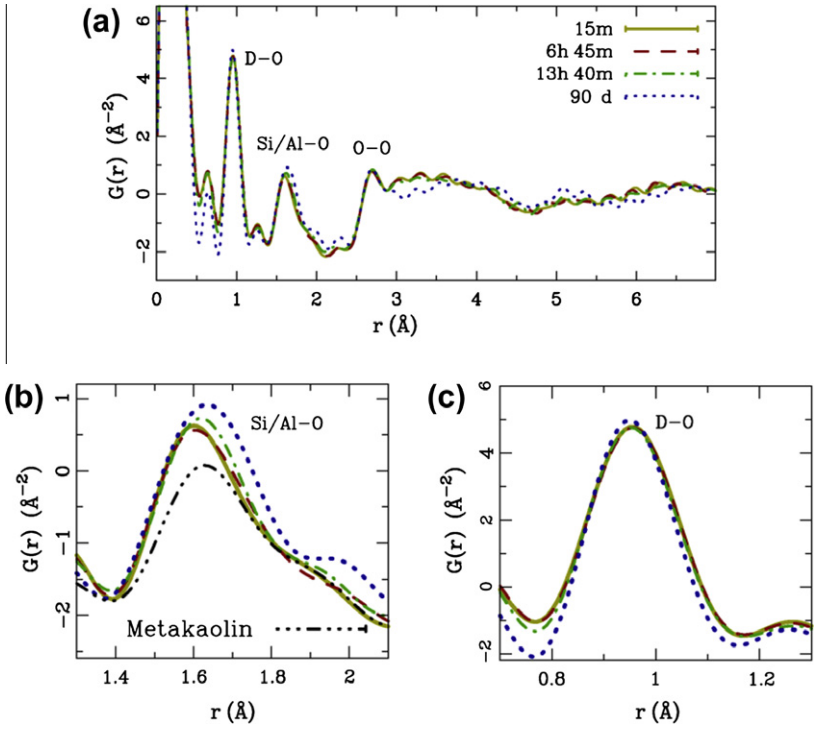

Fig. 2. *In situ* neutron pair distribution functions of a deuterated sodium silicate-activated metakaolin geopolymer, obtained after reaction times as marked, at ambient temperature (25 °C). Parts (b) and (c) are expansions of key peaks in (a) and (b) shows a comparison to the pair distribution function of the raw metakaolin used in geopolymer synthesis. Data from [21], collected using the HIPD instrument at the Lujan Neutron Scattering Center, Los Alamos National Laboratory, New Mexico, USA.

beams interact with low-elemental number solids [32]. Lower electron energies can also be used to minimize this, but at the cost of requiring very careful surface preparation, and reducing the availability of information regarding heavier elements. X-rays are also much more sensitive to the presence of trace elements; the sensitivity of X-ray fluorescence microscopy to the distribution of components present at levels below 0.1 wt.% is valuable in the study of key elements such as Cr in fly ashes [33].

The use of a highly focused X-ray beam enables extremely high-resolution analysis of elemental compositions in the binder structure, as demonstrated in Fig. 3. These images display the Ca and Si concentrations, and the Ca/Si ratios, in a binder region containing two slag particles (Ca-rich regions) embedded in the binder gel.

The data in Fig. 3 provide insight into the chemistry of the binder gel and its interaction with the slag particles. It is seen that the Ca/Si ratio of the outer product gel (which forms in the spaces initially filled by liquid) is notably lower than that of the slag particles, rarely exceeding 1.0 (approximately dark brown on the color scale used here) in the regions of the scan identifiable as being gel, compared to an average value closer to 1.3 (orange on the color scale) in the unreacted slag particles, and much higher than this in some parts of the remnant slag particles in Fig. 3. The gel Ca/Si ratio is relatively homogeneous in the outer product region, while the residual slag particles vary significantly in Ca/Si ratio; the reasons for this apparently incongruent dissolution of the slag particles are unknown. The inner product gel (the gel which fills the spaces initially occupied by particles) is only slightly lower in Ca/Si ratio than the bulk of the slag particles, although has a lower density (due to the presence of porosity and water) and thus has lower concentrations of both Ca and Si than the slag, although the ratio between these two elements is not changed much. The inner and outer product gels have previously been identified to differ in Ca/Si ratio and morphology in alkali-activated binders [30,34], and these data are consistent with those observations.

In obtaining these data, the full X-ray fluorescence spectra for elements Al and heavier on the periodic table are collected, and then the intensities in desired spectral regions integrated to provide the concentrations of each element (see Supporting Information of [33] for a full description of this procedure). Several other elements of interest were identified, in addition to the dominant Ca and Si, in the binder region depicted in Fig. 3, there are several Ti-rich points localized within remnant slag particles, and the elemental maps of S and Mn also correlate closely with the Ca map, indicating the presence of these elements predominantly within the unreacted slag rather than being extensively distributed through the binder. There is not strong evidence of the presence of any metakaolin particles within the region depicted here in Fig. 3, as the Al map corresponding to this region is rather featureless.

However, Fig. 4 does clearly show the presence of a partially-reacted metakaolin particle (identified by high Si, very high Al; moderate Ca) and a partially-reacted slag grain (identified by high Si, moderate Al, also relatively high S and some Mn (data not shown)), in a different sample with similar mix design (different slag source, slightly lower metakaolin content and modulus (activator SiO_2/Na_2O ratio)). This region happens not to contain any unreacted slag particles, although these are visible elsewhere in the same sample [35].

The distribution of Ca within this region is surprisingly uniform, both within and outside the areas identified as having been derived from metakaolin and slag particles (as marked in the Si map). This shows that the ingress of Ca into the region initially filled by a metakaolin particle, forming calcium-alkali-aluminosilicate gel, is more rapid than the dispersion of the Al supplied by the metakaolin throughout the remainder of the binder region. The region at the top of the images shown in Fig. 4 is rich in Ca but relatively poor in Si, with moderate Al content. This is identified as corresponding to inner product gel; the proximity of this gel region to the metakaolin particle has provided additional Al, and the gel

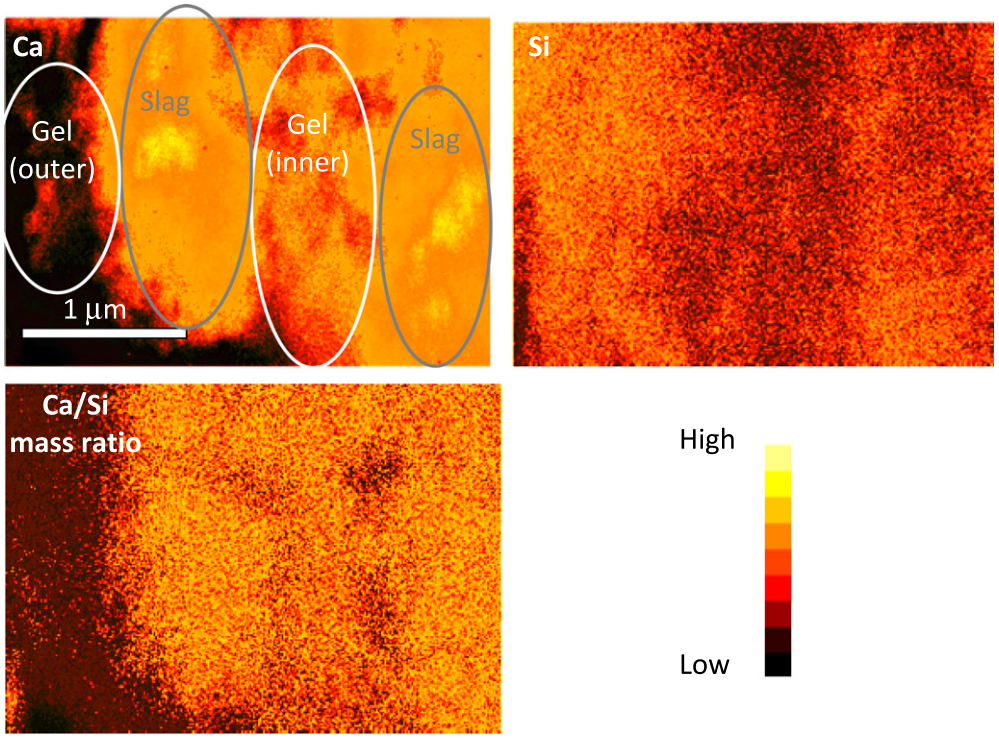

Fig. 3. X-ray fluorescence micrographs of a sodium metasilicate-activated binder (75% slag/25% metakaolin, activator SiO_2/Na_2O ratio 1.0). The maps were obtained with a focused 12 keV X-ray beam with a spot size of 50 nm, and a step size of 10 nm. The same region is shown in all parts of the Figure; the gel and slag regions are identified in the Ca map only. Data were collected using beamline 26-ID (Hard X-ray Nanoprobe), operated by the Center for Nanoscale Materials at the Advanced Photon Source, Argonne National Laboratory, Illinois, USA.

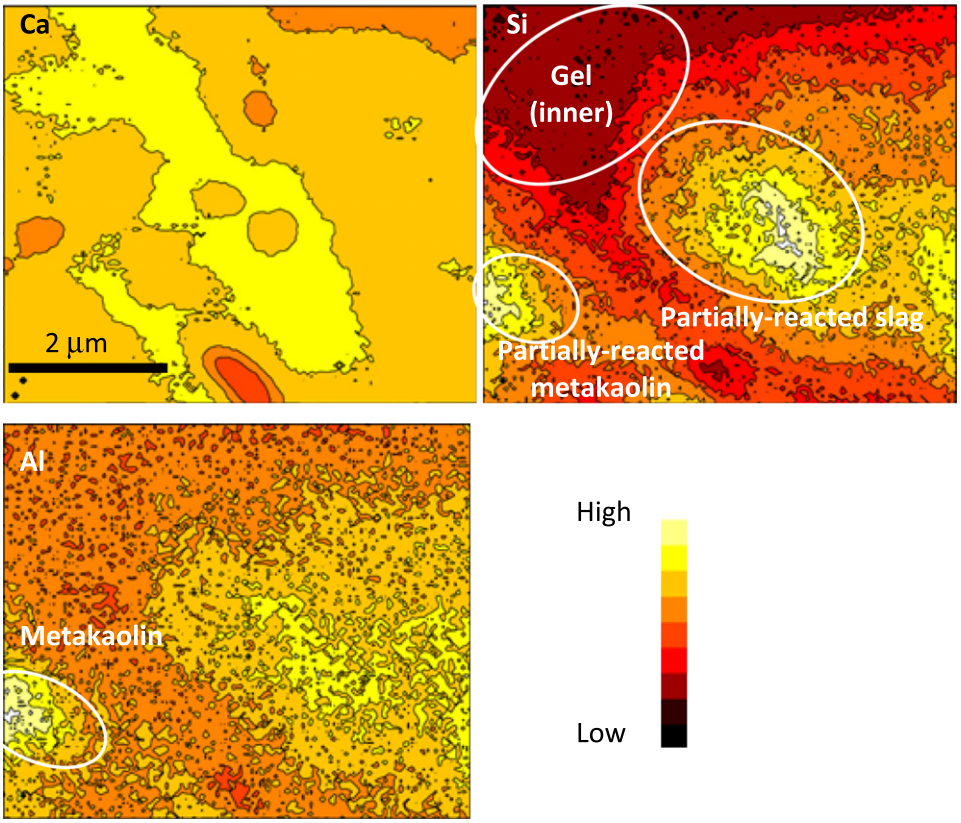

Fig. 4. X-ray fluorescence micrographs of a sodium silicate-activated binder (80% slag/20% metakaolin, activator SiO_2/Na_2O ratio 0.9). The maps were obtained with a focused 10.5 keV X-ray beam with a spot size of 50 nm, and a step size of 50 nm. The same region is shown in all parts of the Figure. Data were collected using beamline 26-ID (Hard X-ray Nanoprobe), operated by the Center for Nanoscale Materials at the Advanced Photon Source, Argonne National Laboratory, Illinois, USA.

formed is thus able to be stabilized at a higher Ca/Si ratio than would be the case further from the metakaolin particle.

This highlights the importance of obtaining data from multiple regions on a sample when using techniques operating on such fine length scales to study highly heterogeneous materials. As the resolution of the technique increases, so does the importance of ensuring that the regions scanned are in some way representative of the sample as a whole; for example, almost any alkali-activated binder will contain regions larger than the scan areas in Figs. 3 and 4 which fall entirely within unreacted particles of raw material, and so it is important to scan a sufficiently large area (and with a sufficiently detailed understanding of the chemistry of both reacted and unreacted phases) to enable accurate analysis of complex samples. Further examples of this requirement will be demonstrated in the following section, which discusses X-ray tomography as applied on different length scales to the analysis of geopolymers.

2.4. X-ray tomography

Fig. 5a shows a region of interest selected from an X-ray microtomographic reconstruction of an alkali-activated slag/metakaolin sample of the same composition as the sample depicted in Fig. 4 [35]; the image shows a region 150 × 150 μm in size, which has been extracted from a reconstructed three-dimensional dataset computed from a set of X-ray transmission images. A grayscale histogram of the volume of interest is presented in Fig. 5b, with distinct peaks due to the reaction products (the peak at a grayscale value of around 70) and unreacted slag (at 170). Fig. 5a shows a clear distinction between inner and outer product regions, with the outer product showing lower X-ray absorption (corresponding to lower Ca/Si ratio) at the solution modulus of 0.9 used here, which is consistent with the discussion presented in Section 2.3. However, these two types of reaction products do not show distinct peaks in the histogram in Fig. 5b. Remnant metakaolin particles are not immediately evident in Fig. 5a, which is consistent with observations elsewhere that these particles are difficult to distinguish from the gel regions of mixed slag–metakaolin binders by X-ray microtomography [36]. It is likely that the metakaolin particles (which are dense but low in elemental number) and the gel (which contains some Ca, the heaviest element present in significant concentrations in the samples, but which is also nanoporous) have a similar X-ray absorption cross-section, and thus they appear similar in the grayscale images obtained from the tomography experiment.

It is also evident that there was some degree of agglomeration of the slag particles prior to reaction, as multiple slag grains (bright, smooth, angular regions in Fig. 5a) are seen to be embedded in the inner product regions. However, some of the larger slag particles are apparently not surrounded by inner product regions, which may indicate differences in reactivity between different grains of the slag. This is to some extent unexpected, as the slag used here is predominantly glassy [37,38], and thus suggests either that there is some degree of differential reactivity between slag particles, or alternatively that the larger non-agglomerated slag particles react more gradually than the agglomerates of finer particles, and thus do not display such marked distinction between inner and outer product regions. Electron microscopy has previously shown Mg-rich, Ca-depleted rims surrounding residual slag grains in alkali-activated slag binders [11]; this is not observed here, possibly due to the low Mg content of the slag used here [37,38]. There are some large pores present in the sample due to air entrainment during molding of the paste specimen studied, while the porosity of the gel itself is too fine to be observed directly by this technique.

The data presented here were collected in absorption contrast mode; phase contrast tomography is also possible, and offers potentially higher sensitivity in systems where absorption contrast is low [39], which means that it is particularly useful in nanotomography experiments [40]. The voxel size of the data shown in Fig. 5 is 750 nm; this is considered to be a relatively high resolution for absorption contrast X-ray tomographic studies of complex materials, as complexities related to both the physics of the experiment and the handling of very large data sets enforce a compromise between voxel size and sample size [41]. The sample size of a cement or alkali-activated binder which is able to be most effectively analyzed using the 750 nm voxel size applied here, using bending magnet radiation from a high-energy synchrotron ring (in the energy range approximately 20–30 keV), is no more than a few millimeters. Neutron tomography is particularly well suited to the analysis of larger specimens, and of the distribution of water within specimens [42], but offers much lower spatial resolution than can be achieved using X-ray tomography due to the difficulties inherent in spatially-resolved detection of neutrons. However, the most important limitations in high-resolution tomography of large samples are currently related to data handling, as a 2048 voxel^3 dataset (i.e. approximately a 1.5 mm cube at 750 nm resolution, corresponding to the size of many detectors used in tomographic

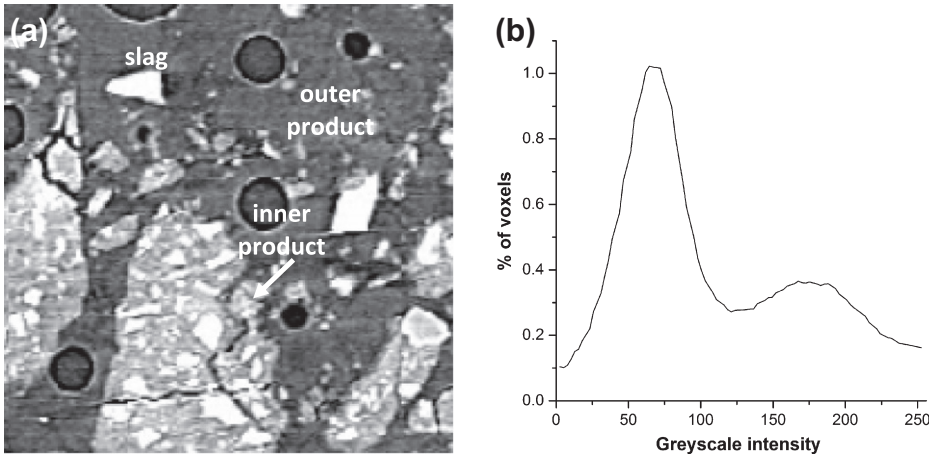

Fig. 5. (a) One slice from an X-ray microtomography scan of a sodium silicate-activated binder (80% slag/20% metakaolin, activator SiO_2/Na_2O ratio 0.9), field of view 150 × 150 μm, and (b) a grayscale histogram of the volume of interest. Data were collected on beamline 2-BM-B at the Advanced Photon Source, Argonne National Laboratory, Illinois, USA, using 22.5 keV radiation.

instruments at present), where each voxel contains 8-bit grayscale information, occupies tens of gigabytes. These datasets can be handled with modern computational infrastructure, and the capabilities of this technique will be expected to continue to grow in line with advances in computational capacity.

It is possible to use tomography to access finer length scales than the 750 nm voxel size depicted in Fig. 5, although at the cost of requiring a very small sample size; data at a spatial resolution below 100 nm have been obtained and published for an alkali-activated fly ash sample [43] using the 'Hard X-ray Nanoprobe' (beamline 26-ID) instrument at the Advanced Photon Source synchrotron, operating in Zernike phase contrast mode. The field of view in that experiment was around 12 μm × 12 μm, meaning that the accessible sample size is less than this. In a tomographic scan, it is important that the whole sample remains within the field of view and depth of focus throughout the experiment, because if part of the sample moves out of the field of view, the reconstruction algorithm is prone to failure for at least a pie-slice shaped region of the sample. This is particularly important for samples (such as cements, and particularly alkali-activated binders with low Ca content) which show relatively low X-ray contrast between regions, because tomographic reconstruction of such samples is always difficult, and may become entirely impossible if some part of the data set is missing. It is a very challenging mechanical engineering problem to achieve the degree of stability required to rotate a sample several microns in size through 180°, in step sizes of around 0.1°, all the time remaining within the field of view of the detector, and while subject to ambient vibrations and/or thermally induced expansion/contraction [44,45]. Nonetheless, both synchrotron and laboratory instruments offering tomography with sub-200 nm spatial resolution are currently available, and the application of high-resolution tomographic methods to the study of cement materials is becoming increasingly widespread and increasingly powerful with advances in computing and beamline technology [46–50]. The coupling of X-ray diffraction and tomographic techniques has also proven valuable in the analysis of key crystal phases within hydrated Portland cements [51]. Alkali-activated binders are in general insufficiently crystalline for such an approach to give immediately comprehensible data, but it may be that developments in the technique and in the understanding of alkali-activated binder chemistry could provide advances in this area in future.

While the qualitative analysis of tomographic data does provide important insight, particularly in the development of an understanding of pore structures and the geometry of the solid phases on a range of length scales, it is also important to be able to obtain quantitative information from the data sets. This necessitates segmentation of the data into regions defined as 'pore' and as 'solid', and the methodologies by which this may be achieved remain the subject of much discussion in the literature. Fig. 6 illustrates part of the difficulty in accurately achieving pore segmentation for samples with a fundamental pore size smaller than the voxel resolution of the data – which will certainly be the case for all microtomographic studies of alkali-activated binders, as the dominant pore size present in these materials (as determined through nitrogen sorption and visible in electron microscopy) is usually in the nanometer range [43,52–56].

The additional difficulty related to the analysis of alkali-activated binders by microtomography is that there is often limited X-ray absorption contrast between the unreacted or partially-reacted raw materials and the newly-formed binder phases [49]. Greyscale histograms of tomographic reconstructions of hydrated Portland cement usually show three distinct peaks, which are assigned to the pores, the hydration products, and the anhydrous cement [47,50]. However, the greyscale histogram of an alkali-activated binder is often unimodal [49,57], which means that it is more difficult to select a threshold value for the binary thresholding into 'pore' and 'solid' regions. This is represented schematically in Fig. 6b by the upper left-hand region, which is 50% solid and 50% pore volume (as seen by comparison with the same sector of Fig. 6a), and is thus not straightforwardly classified as either 'solid' or 'pore' if the threshold is set at a greyscale value halfway between the solid and pore regions. More advanced thresholding algorithms, potentially including the use of edge detection to identify unreacted particles, will be needed to resolve this difficulty, which is inherent in the physics and chemistry of low-Ca aluminosilicate binders, and will also be observed in other cement-type systems where the atomic number densities of some or all of the unreacted phases (fly ash being the particularly problematic case in alkali-activated binders) and of the reaction products are comparable.

2.5. Discussion and perspectives for future work

The combination of X-ray fluorescence microscopy with other analytical techniques, particularly nanoscale [43] and microscale [49] tomographic analysis of the three-dimensional structure of the binder gel, as well as infrared microscopic analysis (on a longer

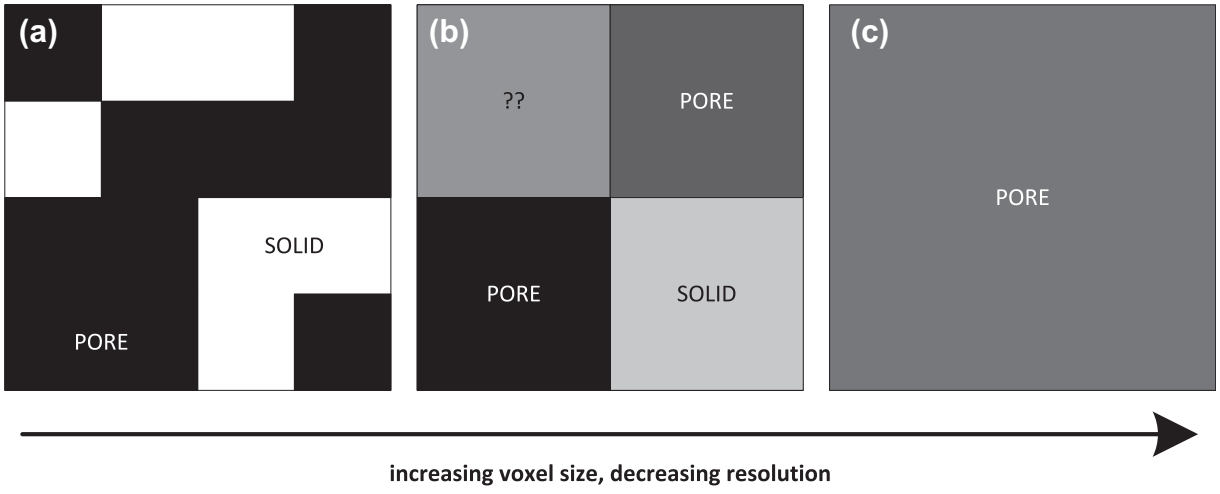

Fig. 6. The distinction between pore space and binder phase becomes more difficult as voxel size is increased above the fundamental pore size, for an arbitrary pore geometry. As the voxel size increases, the likelihood of error associated with segmentation increases; in (a) it is clear what is pore and what is solid, whereas in (b) and (c) it becomes increasingly more difficult to distinguish the pore and solid phases.

length scale) and pair distribution function analysis (on a finer length scale) for chemical bonding information, provides immense power in understanding the development and distribution of gel phases within geopolymer binders. These techniques are almost exclusively available at beamline facilities, although laboratory-scale tomography and pair distribution function facilities are now commercially available, with capabilities approaching those of some lower-end synchrotron sources. Neutron scattering and high-resolution X-ray fluorescence microscopy are likely to remain limited to major beamline facilities, but such facilities are increasing in availability and capabilities worldwide, and provide a good deal of scope for developments in the science of construction materials in coming years. Techniques such as scanning transmission X-ray microscopy (including the capability for spatially resolved X-ray absorption spectroscopy), which has been applied with success to the study of Portland cement and its component phases [58,59], but which have not yet produced publications related to geopolymer materials, will undoubtedly provide additional insight as advances in both instrumentation and scientific understanding of alkali-activated binders enable developments in this area. Cement and geopolymer materials are generally much less susceptible to beam damage effects than is the case for biological materials, and the absorbed doses in all experiments reviewed in this paper were multiple orders of magnitude below the thresholds for degradation quoted for Portland cement-based materials in [60]. However, it may become necessary to be cautious in this regard with future developments in high-intensity radiation sources, or in cases when very long experiment durations are required.

3. Conclusions

The combination of a variety of beamline-based techniques has been shown to provide detailed nanoscale information regarding the chemistry of alkali-activated binders, which has not been accessible through laboratory-based analysis. Synchrotron infrared microscopy has shown the detail of the effects of nanoparticle seeding on geopolymer gel homogeneity at a chemical and microstructural level. *In situ* neutron pair distribution function analysis shows the evolution of both bonding environments in framework and non-framework species during the formation of the geopolymer binder. X-ray fluorescence microscopy provides an understanding of elemental distributions on a length scale as fine as tens of nanometers, while tomography provides the opportunity for three-dimensional reconstruction of the distribution of pore and solid phases. Each of these techniques in isolation is powerful, but by combining the data available through *in situ* and *ex situ* analysis and across a wide range of length scales, a more holistic understanding of the binder structure can be obtained.

In developing future work in this area, it is likely that the most important information will be gained by the combination of various techniques to provide simultaneous multi-technique characterization of samples. Approaches involving combinations of complementary techniques, such as tomography with elemental specificity, or spatially-resolved spectroscopy (as in the infrared microscopy presented here), are likely to provide the key advances in this area. The ongoing developments in data acquisition [61,62] and handling [63,64] which are beginning to make available *in situ* analysis of reaction processes by advanced techniques (as in the PDF work discussed here) will provide powerful analytical capabilities, and these data will then require detailed conceptual and/or kinetic modeling to provide a detailed understanding of the key features of the data sets. It is becoming increasingly uncommon for a single technique, used in isolation, to provide important new insight into the structure or chemistry of a complex material system such as an alkali-activated binder; complementary studies provide unparalleled power and depth of analysis which cannot often be achieved from a single technique.

Acknowledgements

The program of work summarized in this paper has been funded through grants from the Australian Research Council, including some support via the Particulate Fluids Processing Centre, as well as through a Linkage Grant co-sponsored by Zeobond Pty Ltd. The infrared miscroscopy component of this research was undertaken on the IR beamline at the Australian Synchrotron, Victoria, Australia. This work has also benefited from the use of HIPD at the Lujan Center at Los Alamos Neutron Science Center, funded by the DOE Office of Basic Energy Sciences. The participation of CEW and AL in this work was supported by Los Alamos National Laboratory. Los Alamos National Laboratory is operated by Los Alamos National Security LLC under DOE Contract DE-AC52-06NA25396. CEW gratefully acknowledges the support of the U.S. Department of Energy through the LANL/LDRD Program. Use of the Advanced Photon Source and the Center for Nanoscale Materials was supported by the U.S. Department of Energy, Office of Science, Office of Basic Energy Sciences, under Contract No. DE-AC02-06CH11357. Travel funding for experimental work was provided by the Brian Robinson Fellowship awarded to JLP, as well as through the Australian Synchrotron International Access Program, and through the Access to Major Research Facilities Program administered by ANSTO. The authors thank Dr. Hyunjeong Kim, Dr. Mark Tobin, Dr. Ljiljana Puskar and Dr. Katherine Page for assistance with experimental work.

References

[1] Meral C, Benmore CJ, Monteiro PJM. The study of disorder and nanocrystallinity in C–S–H, supplementary cementitious materials and geopolymers using pair distribution function analysis. Cem Concr Res 2011;41:696–710.
[2] Provis JL, Lukey GC, van Deventer JSJ. Do geopolymers actually contain nanocrystalline zeolites? A reexamination of existing results. Chem Mater 2005;17:3075–85.
[3] van Deventer JSJ, Provis JL, Duxson P. Technical and commercial progress in the adoption of geopolymer cement. Miner Eng 2012;29:89–104.
[4] Shi C, Krivenko PV, Roy DM. Alkali-activated cements and concretes. Abingdon (UK): Taylor & Francis; 2006.
[5] van Deventer JSJ, Provis JL, Duxson P, Brice DG. Chemical research and climate change as drivers in the commercial adoption of alkali activated materials. Waste Biomass Valoriz 2010;1:145–55.
[6] Creagh D, McKinlay J, Dumas P. The design of the infrared beamline at the Australian synchrotron. Vibr Spectrosc 2006;41:213–20.
[7] Fernández-Jiménez A, Palomo A. Mid-infrared spectroscopic studies of alkali-activated fly ash structure. Micropor Mesopor Mater 2005;86:207–14.
[8] Rees CA, Provis JL, Lukey GC, van Deventer JSJ. Attenuated total reflectance fourier transform infrared analysis of fly ash geopolymer gel aging. Langmuir 2007;23:8170–9.
[9] Lee WKW, van Deventer JSJ. Use of infrared spectroscopy to study geopolymerization of heterogeneous amorphous aluminosilicates. Langmuir 2003;19:8726–34.
[10] Rees CA, Provis JL, Lukey GC, van Deventer JSJ. The mechanism of geopolymer gel formation investigated through seeded nucleation. Colloids Surf A 2008;318:97–105.
[11] Lloyd RR, Provis JL, van Deventer JSJ. Microscopy and microanalysis of inorganic polymer cements. 2: The gel binder. J Mater Sci 2009;44:620–31.
[12] Hajimohammadi A, Provis JL, van Deventer JSJ. The effect of silica availability on the mechanism of geopolymerisation. Cem Concr Res 2011;41:210–6.
[13] Hajimohammadi A, Provis JL, van Deventer JSJ. The effect of alumina release rate on the mechanism of geopolymer gel formation. Chem Mater 2010;22:5199–208.
[14] Hajimohammadi A, Provis JL, van Deventer JSJ. Time-resolved and spatially-resolved infrared spectroscopic observation of seeded nucleation controlling geopolymer gel formation. J Colloid Interf Sci 2011;357:384–92.
[15] Egami T, Billinge SJL. Underneath the bragg peaks: structural analysis of complex materials. Oxford: Plenum; 2003.
[16] Proffen T, Billinge SJL, Egami T, Louca D. Structural analysis of complex materials using the atomic pair distribution function – a practical guide. Z Kristallogr 2003;218:132–43.
[17] White CE. Pair distribution function analysis of amorphous geopolymer precursors and binders: the importance of complementary molecular simulation. Z Kristallogr 2012;227:304–12.

[18] Bell JL, Sarin P, Provis JL, Haggerty RP, Driemeyer PE, Chupas PJ, et al. Atomic structure of a cesium aluminosilicate geopolymer: a pair distribution function study. Chem Mater 2008;20:4768–76.
[19] Bell JL, Sarin P, Driemeyer PE, Haggerty RP, Chupas PJ, Kriven WM. X-ray pair distribution function analysis of a metakaolin-based, $KAlSi_2O_6{\cdot}5.5H_2O$ inorganic polymer (geopolymer). J Mater Chem 2008;18:5974–81.
[20] White CE, Provis JL, Proffen T, van Deventer JSJ. The effects of temperature on the local structure of metakaolin-based geopolymer binder: a neutron pair distribution function investigation. J Am Ceram Soc 2010;93:3486–92.
[21] White CE, Provis JL, Llobet A, Proffen T, van Deventer JSJ. Evolution of local structure in geopolymer gels: an *in situ* neutron pair distribution function analysis. J Am Ceram Soc 2011;94:3532–9.
[22] Provis JL, van Deventer JSJ. Direct measurement of the kinetics of geopolymerisation by *in situ* energy dispersive X-ray diffractometry. J Mater Sci 2007;42:2974–81.
[23] Provis JL, van Deventer JSJ. Geopolymerisation kinetics. 1. In situ energy dispersive X-ray diffractometry. Chem Eng Sci 2007;62:2309–17.
[24] White CE, Bloomer B, Provis JL, Henson NJ, Page K. The synergy between total scattering and advanced simulation techniques in understanding geopolymer gel evolution: quantifying extent of reaction using *in situ* X-ray pair distribution function analysis. In: Proceedings of NICOM4. Agios Nikolaos, Greece; 2012 [CD-ROM].
[25] White CE, Provis JL, Proffen T, Riley DP, van Deventer JSJ. Combining density functional theory (DFT) and pair distribution function (PDF) analysis to solve the structure of metastable materials: the case of metakaolin. Phys Chem Chem Phys 2010;12:3239–45.
[26] White CE, Provis JL, Proffen T, Riley DP, van Deventer JSJ. Density functional modeling of the local structure of kaolinite subjected to thermal dehydroxylation. J Phys Chem A 2010;114:4988–96.
[27] Duxson P, Lukey GC, Separovic F, van Deventer JSJ. The effect of alkali cations on aluminum incorporation in geopolymeric gels. Ind Eng Chem Res 2005;44:832–9.
[28] Davidovits J. Geopolymer chemistry and applications. Saint-Quentin (France): Institut Géopolymère; 2008.
[29] Le Saoût G, Ben Haha M, Winnefeld F, Lothenbach B. Hydration degree of alkali-activated slags: a ^{29}Si NMR study. J Am Ceram Soc 2011;94:4541–7.
[30] Richardson IG, Brough AR, Groves GW, Dobson CM. The characterization of hardened alkali-activated blast-furnace slag pastes and the nature of the calcium silicate hydrate (C–S–H) paste. Cem Concr Res 1994;24:813–29.
[31] Richardson IG, Skibsted J, Black L, Kirkpatrick RJ. Characterisation of cement hydrate phases by TEM, NMR and raman spectroscopy. Adv Cem Res 2010;22:233–48.
[32] Lloyd RR, Provis JL, van Deventer JSJ. Microscopy and microanalysis of inorganic polymer cements. 1: Remnant fly ash particles. J Mater Sci 2009;44:608–19.
[33] Provis JL, Rose V, Bernal SA, van Deventer JSJ. High resolution nanoprobe X-ray fluorescence characterization of heterogeneous calcium and heavy metal distributions in alkali activated fly ash. Langmuir 2009;25:11897–904.
[34] Xu H, Provis JL, van Deventer JSJ, Krivenko PV. Characterization of aged slag concretes. ACI Mater J 2008;105:131–9.
[35] Bernal SA. Carbonatación de concretos producidos en sistemas binarios de una escoria siderúrgica y un metacaolín activados alcalinamente. Escuela de Ingeniera de Materiales. Cali, Colombia: Universidad del Valle; 2009.
[36] Gordon LE, Myers RJ, Cao L, Provis JL, Van Deventer JSJ. Determination of the pore structure of alkali activated aluminosilicate systems exposed to carbon capture solvents. In: 31st Cement and concrete science conference. Novel developments and innovation in cementitious materials. London, (UK) : Imperial College; 2011 [CD-ROM].
[37] Bernal SA, Mejía de Gutierrez R, Rose V, Provis JL. Effect of silicate modulus and metakaolin incorporation on the carbonation of alkali silicate-activated slags. Cem Concr Res 2010;40:898–907.
[38] Bernal SA, Provis JL, Mejía de Gutierrez R, Rose V. Evolution of binder structure in sodium silicate-activated slag–metakaolin blends. Cem Concr Compos 2011;33:46–54.
[39] Monteiro PJM, Kirchheim AP, Chae S, Fischer P, MacDowell AA, Schaible E, et al. Characterizing the nano and micro structure of concrete to improve its durability. Cem Concr Compos 2009;31:577–84.
[40] Stampanoni M, Mokso R, Marone F, Vila-Comamala J, Gorelick S, Trtik P, et al. Phase-contrast tomography at the nanoscale using hard X rays. Phys Rev B 2010;81:140105.
[41] Cnudde V, Boone M, Dewanckele J, Dierick M, Van Hoorebeke L, Jacobs P. 3D characterization of sandstone by means of X-ray computed tomography. Geosphere 2011;7:54–61.
[42] Brew DRM, de Beer FC, Radebe MJ, Nshimirimana R, McGlinn PJ, Aldridge LP, et al. Water transport through cement-based barriers—a preliminary study using neutron radiography and tomography. Nucl Instr Meth Phys Res A 2009;605:163–6.
[43] Provis JL, Rose V, Winarski RP, van Deventer JSJ. Hard X-ray nanotomography of amorphous aluminosilicate cements. Scripta Mater 2011;65:316–9.
[44] Maser J, Winarski R, Holt M, Shu D, Benson C, Tieman B, Preissner C, Smolyanitskiy A, Lai B, Vogt S, Wiemerslage G, Stephenson GB. The hard X-ray nanoprobe beamline at the advanced photon source. In: Proceedings of the 8th international conference on X-ray microscopy. Himeji, Japan; 2005. p. 26–9.
[45] Shu D, Maser J, Holt M, Winarski R, Preissner C, Smolyanitskiy A, et al. Optomechanical design of a hard X-ray nanoprobe instrument with nanometer-scale active vibration control. AIP Conf Proc 2007;879:1321–4.
[46] Diamond S, Landis EN. Microstructural features of a mortar as seen by computed microtomography. Mater Struct 2007;40:989–93.
[47] Gallucci E, Scrivener K, Groso A, Stampanoni M, Margaritondo G. 3D experimental investigation of the microstructure of cement pastes using synchrotron X-ray microtomography (μCT). Cem Concr Res 2007;37:360–8.
[48] Helfen L, Dehn E, Mikulik P, Baumbach T. Three-dimensional imaging of cement microstructure evolution during hydration. Adv Cem Res 2005;17:103–11.
[49] Provis JL, Myers RJ, White CE, Rose V, van Deventer JSJ. X-ray microtomography shows pore structure and tortuosity in alkali-activated binders. Cem Concr Res 2012;42:855–64.
[50] Promentilla MAB, Sugiyama T, Hitomi T, Takeda N. Quantification of tortuosity in hardened cement pastes using synchrotron-based X-ray computed microtomography. Cem Concr Res 2009;39:548–57.
[51] Valentini L, Dalconi MC, Parisatto M, Cruciani G, Artioli G. Towards three-dimensional quantitative reconstruction of cement microstructure by X-ray diffraction microtomography. J Appl Cryst 2011;44:272–80.
[52] Sindhunata, Provis JL, Lukey GC, Xu H, van Deventer JSJ. Structural evolution of fly ash-based geopolymers in alkaline environments. Ind Eng Chem Res 2008;47:2991–9.
[53] Lloyd RR, Provis JL, Smeaton KJ, van Deventer JSJ. Spatial distribution of pores in fly ash-based inorganic polymer gels visualised by wood's metal intrusion. Micropor Mesopor Mater 2009;126:32–9.
[54] Collins F, Sanjayan JG. Effect of pore size distribution on drying shrinking of alkali-activated slag concrete. Cem Concr Res 2000;30:1401–6.
[55] Collins F, Sanjayan J. Prediction of capillary transport of alkali activated slag cementitious binders under unsaturated conditions by elliptical pore shape modeling. J Porous Mater 2010;17:435–42.
[56] Shi C. Strength, pore structure and permeability of alkali-activated slag mortars. Cem Concr Res 1996;26:1789–99.
[57] Provis JL, van Deventer JSJ. Tailoring geopolymer structure to improve material performance. In: First international conference on advances in chemically-activated materials. Jinan, China; 2010. p. 58–65.
[58] Kirchheim AP, Dal Molin DC, Fischer P, Emwas A-H, Provis JL, Monteiro PJM. Real-time high-resolution X-ray imaging and nuclear magnetic resonance study of the hydration of pure and Na-doped C_3A in the presence of sulfates. Inorg Chem 2011;50:1203–12.
[59] Ha J, Chae S, Chou K, Tyliszczak T, Monteiro P. Effect of polymers on the nanostructure and on the carbonation of calcium silicate hydrates: a scanning transmission X-ray microscopy study. J Mater Sci 2012;47:976–89.
[60] Acevedo CE, Serrato MG. Determining the effects of radiation on aging concrete structures of nuclear reactors. In: WM2010 conference. Tucson, AZ; 2010 [CD-ROM proceedings, Paper 10243].
[61] Kaestner AP, Munch B, Trtik P. Spatiotemporal computed tomography of dynamic processes. Opt Eng 2011;50:123201.
[62] Momose A, Yashiro W, Harasse S, Kuwabara H. Four-dimensional X-ray phase tomography with talbot interferometry and white synchrotron radiation: dynamic observation of a living worm. Opt Express 2011;19:8423–32.
[63] Cloetens P. Tomography data processing and management. In: ESRF synchrotron grid workshop. Grenoble, France; 2008 <http://www.esrf.eu/events/conferences/esrf-up-work-package-11/presentations/P.CloetenswebSR_grid_computing.pdf>.
[64] Titarenko S, Titarenko V, Kyrieleis A, Withers PJ, De Carlo F. Suppression of ring artefacts when tomographing anisotropically attenuating samples. J Synchr Rad 2011;18:427–35.